J. Appl. Comput. Mech., 11(1) (2025) 239-252
DOI: 10.22055/jacm.2024.46544.4548

ISSN: 2383-4536
jacm.scu.ac.ir

Shahid Chamran
University of Ahvaz

Journal of
Applied and Computational Mechanics

Research Paper

Thermal Heat Transfer Enhancement Analysis of Magnetic Ternary Hybrid Nanofluid in a Hexagonal Cavity with Square Obstacle

Arasukumar Thilagavathi, Vallampati Ramachandra Prasad

Department of Mathematics, Vellore Institute of Technology, Vellore, Tamilnadu- 632014, India,
Email: thilagavathi.a2020@vitstudent.ac.in (T.A.); rcpmaths@gmail.com (V.R.P.)

Received April 08 2024; Revised June 28 2024; Accepted for publication July 05 2024.
Corresponding author: V. Ramachandra Prasad (rcpmaths@gmail.com)
© 2024 Published by Shahid Chamran University of Ahvaz

Abstract. This study aims to explore the natural convection, magnetohydrodynamics and ternary nanofluids containing Fe_3O_4, Cu and TiO_2 in water-ethylene glycol within a hexagonal cavity containing a square obstacle. The Finite element method is utilized through the COMSOL Multiphysics 6.1 software. By utilizing visual representations, the influence of key variables on flow patterns, temperature distribution, and local Nusselt number is effectively illustrated. Simulations were carried out with Rayleigh number ranging from 10^3 to 10^5, heat source and absorption coefficients ranging from -5 to 15, and Hartmann numbers of 0, 70 and 90. The Prandtl number for ethylene glycol is 29.86. The findings of this research confirm that the proper incorporation of nanoparticles significantly enhances the heat transfer properties of base fluids.

Keywords: Natural convection, Hexagonal cavity, Ternary hybrid nanofluid, MHD, Heat generation/absorption, COMSOL multiphysics.

1. Introduction

Natural convection (NC) is of utmost importance in heat transfer processes, exerting an influence on diverse engineering applications. In this research, the intricate dynamics of NC within a hexagonal chamber with a square obstacle are thoroughly examined. The study incorporates the utilization of ternary hybrid nanofluid, an advanced heat transfer fluid, and introduces the added complexity of magneto-hydrodynamics (MHD). The main objective of this research is to enhance our comprehension of the exchange of heat phenomena in geometry, which can offer valuable insights for real-world applications. Ternary hybrid nanofluids, a relatively new advancement, comprise a fusion of three distinct nanoparticles within a base fluid. The complex interaction among these constituents leads to improved thermal characteristics. The paper provides a comprehensive review of the key findings from previous studies on ternary hybrid nanofluids and their influence on heat transfer. This review sets the foundation for the subsequent numerical investigation that will be presented in the later sections of the paper. The inclusion of MHD incorporates magnetic fields as an influential element in the dynamics of fluids. The selection of cavity shape has a substantial effect on the transportation of heat properties. A thorough analysis of relevant scientific literature is reviewed to explore the impact of similar geometries on NC heat transmission. This literature review aims to provide an overview of the studies related to natural convection heat transfer involving ternary hybrid nanofluids in the presence of MHD within a hexagonal block containing a square obstacle.

Hexagonal cavities with square obstacles are of interest in various real-world applications due to their unique geometric and fluid dynamic properties. One prominent application is in the design of heat exchangers, particularly in industries requiring efficient thermal management, such as aerospace, automotive, and electronics cooling. The combination of a hexagonal cavity and a square obstacle enhances heat transfer by promoting complex flow patterns and turbulence, which can significantly improve the heat exchange efficiency. Moreover, in the realm of material science, these structures are utilized in the development of novel metamaterials. Metamaterials with hexagonal cavities and embedded obstacles exhibit unique electromagnetic properties not found in natural materials, leading to advancements in cloaking devices, antennas, and sensors.

In their investigation, Eftekhari et al. [1] examined the impact of the volume fraction, temperature and shear rates. To conduct their work, they employed an Artificial Neural Network (ANN). The research showcases the capability of ANN's to accurately simulate the intricate behavior of Al_2O_3/EG-Water nanofluids by utilizing various training techniques and geometric setups, offering a dependable and effective predictive solution. The utilization of a modified homotopy analysis approach was examined by Afzal et al. [2] in their discussion on steady flow on a stretching surface. It delves into the potential of hybrid nanofluids in boosting heat transportation effectiveness in engine oils. Through the integration of nanoparticles into the oil, the research seeks to elevate thermal conductivity and overall energy distribution efficiency. Utilizing an entropy optimization method, the study assesses and fine-tunes the thermodynamic efficiency of the hybrid nanofluids in combustive engines. Findings reveal notable advancements

Published online: July 20 2024

in energy transmission and energy efficiency, underscoring the promising utility of hybrid nanofluids in augmenting engine performance and curbing thermal losses. Javed et al. [3] investigated the energy transfer occurring in a trapezoidal chamber with inclined walls. The researchers conducted experiments using a lid driven approach and analyzed the movement of liquid within the chamber. Furthermore, they used an increase in the constant Prandtl number across all three inclined angles. In their study, Teamah et al. [4] presented findings indicating that the inclusion of nanoparticles is essential to improve the exchange of energy in the presence of a weak magnetic field. However, when dealing with a strong magnetic field, the use of nanoparticles becomes unnecessary as it leads to a decrease in the transportation of heat. This observation was made within the NC applied geometry. Mansour et al. [5] discovered a decrease in entropy generation as *Ha* decreases and an increase in entropy generation with the value of the nanoparticle volume fraction ϕ. A thorough comparison between previously published studies and their findings reveals a remarkable level of concordance. The results offer a comprehensive analysis of entropy engendering by considering the *Ha*, nanoparticle volume fraction, and various geometric parameters associated with the chamber. An upwind scheme has been used to find the solution. The investigation conducted by Nisar et al. [6] explores the various applications of ferro liquids and hybrid-based liquids. Their research findings indicate that the radiation and temperature ratio parameters contribute to an enhancement in temperature in both flows.

Saranya et al. [7] examined the boundary layer flow in the hybrid ferrofluid. To conduct their research, they utilized a heated cone. The findings revealed that the hybrid ferrofluid exhibited higher skin friction and exchange of energy capabilities compared to both base fluids and simple nanofluids. The enhancement of thermal properties in advanced cooling systems is achieved by combining base fluids with magnetic nanoparticles. In order to comprehend the impact of the rotation and energy transfer characteristics of the spinning cone on liquid behavior, numerical simulations are utilized in this study. The results indicate that the hybrid ferrofluid greatly enhances heat distribution efficiency when compared to traditional liquids. These findings offer valuable insights for various applications such as thermal management, magnetic field manipulation, and engineering systems that necessitate efficient heat dissipation. Das et al. [8] analyzed the effects of rotating hybrid liquid motion in a gyrating channel. The base fluid employed was a mixture of water and EG. The analysis revealed that the temperature distribution increased with the chemical reaction parameter and Dufour number. However, it decreased with the radiation and frequency parameters. The researchers concluded that the introduction of two nanoparticles instead of one nanoparticle resulted in a noteworthy enhancement in the thermal characteristics of the base liquid mixture. Bejan and Khairy [9] examined the phenomenon of NC occurring in a square chamber and featuring an obstacle positioned at its center. Through their investigation, it was discovered that the transfer of heat within the system was notably affected by both the dimensions and orientation of the obstacle. The annulus of different obstacles investigated by Yuan et al. [10] has been studied under the condition of constant temperature and natural convection. A simulation of this phenomenon has been conducted using the SPH method. The study examines the phenomenon of free convection within concentric annuli of varying inner shape in a horizontal orientation. The simulation is classified into four distinct groups, each characterized by the shape of the inner entity. Oztop et al. [11] tackled the numerical study of NC in rectangular block filled with nanoliquids. The study addressed challenges associated with accurately simulating nanofluid behavior and highlighted the importance of proper modeling techniques. The outcomes indicate that nanofluids greatly improve the rate of heat transportation in comparison to traditional fluids, thanks to their exceptional thermal conductivity. These findings provide valuable knowledge for optimizing thermal management systems in engineering applications. By showcasing enhanced convection performance with nanofluids, this study underscores their potential to enhance efficiency in cooling technologies and other systems that necessitate effective heat dissipation.

Ul Haq et al. [12] investigated heat transportation in the corrugated rectangular chamber. The chamber was filled with a porous medium. The FEM was used for dimensionless form. Their research examines the impact of magnetic fields and corrugated geometry on the movement of liquid and energy distribution. The findings indicate that the introduction of a magnetic field and porous medium can greatly modify convection patterns, leading to improved heat transfer efficiency. This study offers valuable information about the development of sophisticated cooling systems and industrial procedures, highlighting the effectiveness of MHD methods in enhancing thermal regulation in intricate geometries. In their research paper, Anandalakshmi et al. [13] studied the transference of thermal energy using porous media within a cavity of a right-angled triangular shape. Their investigation has been based on Bejan's headlines concept. Increased convection at elevated Da levels has a notable impact on the distribution of heat flow, as evident from the high local Nusselt numbers. The heatlines depict the heat transmission for different fluids with various Pr values at high Da, and such an assessment proves advantageous in determining the best design strategy for the thermal management of cavities. In their study, Sheikhzadeh et al. [14] examined a square chamber with side walls containing active portions. The numerical simulation employed FVM, and the enclosure was filled with nanofluid. The study explores how the enhanced thermal properties of nanofluids influence convection patterns and heat transfer efficiency. The findings indicate that the Cu-water nanofluid significantly enhances the transportation of heat when compared to conventional fluids, particularly in systems with partially active heating. These results provide valuable insights for optimizing thermal management systems, showcasing the potential of nanofluids to improve cooling performance in engineering and industrial applications. In their study, Zahan et al. [15] examined the efficacy of various base fluid mixtures of water-ethylene glycol with teri-hybrid nanoparticles, for investigating the movement inside the CD nozzle. The finite element method was employed for their analysis. Comparing different combinations, it was found that the EG-Co-Ag-Zn nanofluid displayed the highest transmission of heat [16-19].

Vinodhini et al. [20] investigated the effects of an oblique magnetic field, heat generation/sink, and complex wall conditions on the magnetoconvective flow of a Buongiorno nanofluid in a rectangular enclosure. The study found that the oblique magnetic field can suppress the flow and heat transfer, and that heat generation can enhance heat transfer while heat absorption can suppress it. Vinodhini et al. [21] studied the effects of viscous dissipation on the NC of an Ag-water nanofluid in a square chamber with a porous medium and complex wall conditions. The findings underscore notable improvements in the transfer of heat and the movement of liquids, which are essential for maximizing the efficiency of thermal control in porous materials and other relevant industrial uses. The impact of implementing a Cattaneo-Christov heat flow model [22] on the flow and heat transfer of a magneto-hybrid nanofluid in a porous square enclosure was examined by Vinodhini et al. [23]. Analysis reveals that the utilization of the Cattaneo-Christov model can lead to notable effects on the outcomes, particularly under elevated temperatures [24, 25].

In research conducted by Khademi et al. [26], various methods were explored to improve heat transfer efficiency in thermal energy storage systems. The study compared the use of an auxiliary fluid with nano-phase change material (nano-PCM) in an inclined enclosure. The main objective was to identify the method that provides better heat transfer properties. The auxiliary fluid method involves the circulation of a secondary fluid (such as water or oil) that absorbs and transfers heat within the enclosure. This approach was contrasted with nano-PCM, which stores and releases thermal energy through phase changes. In summary, this comparative analysis offers valuable insights into enhancing thermal energy storage systems by emphasizing the benefits of using auxiliary fluids instead of nano-PCM in inclined enclosures. These findings have the potential to influence future research and practical applications in energy-efficient thermal management systems. Abtahi Mehrjardi et al. [27] investigated the impact of phase change material ratios and auxiliary fluids on the storage and release of thermal energy. Through testing and modeling, they found that adjusting the PCM ratios significantly affects energy storage rates. The use of auxiliary fluids also improves heat transfer, optimizing the performance of latent heat storage systems. These findings are valuable for developing more efficient energy storage technologies. In [28], it was shown that numerical investigation, sought to improve the efficiency of melting phase change materials (PCMs) by incorporating them with supplementary fluids. They conducted simulations to examine the impact of various parameters on the melting process of PCMs and their ability to store thermal energy. Through the analysis of temperature distributions and heat transfer rates using computational models, they aimed to optimize this procedure. The outcomes of their study provide valuable insights into enhancing the performance of thermal energy storage systems, highlighting the significance of auxiliary fluids in maximizing energy efficiency during phase transitions in PCM-based systems.

Khademi et al. [29] conducted a study on improving thermal efficiency by examining the integration of phase change materials (PCMs) into Brayton cycles. The researchers specifically investigated how PCMs could enhance heat transfer processes and increase energy efficiency in the cycle. Through the analysis of computational models, they evaluated the influence of PCM properties and configurations on the performance of the system. The results of their study emphasize the potential of PCMs to improve heat transfer and overall efficiency in Brayton cycles. These findings provide valuable insights for the advancement of sustainable energy technologies, as PCMs have the ability to effectively store and release thermal energy in high-temperature applications. Amiri Delouei et al. [30] explored active methods to enhance heat transfer in city gate station indirect heaters. The study focused on improving thermal efficiency through practical applications and real-world performance. By conducting experiments and modeling scenarios, they evaluated the effectiveness of different heat transfer enhancement strategies. Their findings offer valuable insights into optimizing city gate station operations using advanced heat transfer techniques, contributing to more efficient energy distribution systems. Hedeshi et al. [31] involved an examination of nanofluids as the working fluid in an ultrasonic-assisted double-pipe counter-flow heat exchanger. The study focused on determining how the inclusion of nanoparticles in fluids can improve heat transfer efficiency within this particular setup. By conducting experiments and analyzing various factors such as heat transfer coefficients and thermal performance enhancements, the researchers were able to highlight the potential of nanofluids in enhancing heat exchange processes in ultrasonic-assisted heat exchangers. This research offers promising possibilities for the development of more efficient thermal management systems.

Abaszadeh et al. [32] utilized an immersed boundary–lattice Boltzmann method to investigate radiative heat transfer in irregular two-dimensional geometries. Their research delved into the potential of this computational technique to effectively replicate intricate heat transfer behaviors in unconventional shapes. Through a concentrated effort on numerical modeling and thorough examination, the team sought to gain a deeper understanding of the complex relationship between radiation and geometry. The findings of their investigation offer significant perspectives on enhancing heat transfer mechanisms in various industrial and environmental settings using sophisticated computational methodologies. The work done by Abaszadeh et al. [33] presented a new computational method that combines the Immersed Boundary Method (IBM) and the Lattice Boltzmann Method (LBM) to tackle the simulation of thermal radiation in complex geometries. Traditional approaches often struggle with accurately representing irregular boundaries and intricate thermal interactions. By integrating IBM, which is effective at handling irregular geometries, with LBM, known for its efficiency in fluid dynamics simulations, this study introduces a hybrid framework that improves accuracy and computational efficiency. The direct-forcing technique within IBM stands out for its precise imposition of boundary conditions without the need for complex meshing, making it well-suited for irregular domains. This development offers a powerful tool for researchers and engineers working on thermal radiation issues in various scientific and engineering fields, providing better performance compared to conventional methods.

Iron (III) oxide is useful in diagnostics in clinical applications, aerospace technology, magnetic data storage, food and agriculture, electronics, coatings and environmental remediation. Moreover, ferric oxide is used in contrast agents for Magnetic Resonance Imaging, nanowires, gene carriers for gene therapy, automotive, therapeutic agents for hyperthermia-based cancer treatments and nanofibers. The purification of air is of the utmost importance for all living organisms, and one way this is achieved is through the oxidation of indoor air pollutants using TiO_2 nanoparticles. TiO_2 is also found in various food products such as white-colored sauces, confectioneries, nondairy creamers, and cheese. Additionally, the biosynthesis of TiO_2 nanoparticles is a key area of focus, along with their application in industries like pharmaceuticals, construction, textiles and food. The implementation of nano TiO_2 photocatalyst coating will serve as an imperceptible layer and can be administered on various surfaces such as ceilings, car interiors, curtains, and floor carpets. The utility of TiO_2 nanoparticles finds its purpose in diverse domains including aerospace, solar cells and agriculture. Copper wire is used in power generation, electronic circuitry and power distribution for telecommunications, power transmission. Copper kitchenware is favored by individuals due to its appealing look and its ability to inhibit the growth of bacteria. Businesses also utilize copper piping to ensure the cleanliness and bacteria-free state of various liquids, like water or oil. Furthermore, in ancient times, individuals who couldn't afford gold jewelry opted for copper, due to its flexible design. The high electrical conductivity of copper makes it a popular choice for wiring purposes. Additionally, copper finds application in construction tools and various gadgets, such as screwdrivers, wrenches, and pliers.

A significant research void exists in the realm of numerical simulation of natural convection in MHD filled heat source and sink with ternary hybrid nanofluid (Fe_3O_4-Cu-TiO_2 with EG-water base fluid) within a hexagonal cavity containing an obstacle. This void is primarily due to the lack of comprehensive investigations that consider the combined effects of MHD, heat source and sink, ternary hybrid nanofluids, and complex cavity geometries using the COMSOL Multiphysics software with the FEM method. This study primarily focuses on analyzing the utilization of water-ethylene glycol as a base fluid and its interaction with ternary nanofluid in the obstruction contained in a chamber. Addressing this gap is crucial for advancing our understanding of convective heat transfer phenomena and facilitating the development of more accurate predictive models for various engineering applications.

2. Mathematical Formulation

The hexagonal region with a square obstacle is taken into consideration in this study, as depicted in Fig. 1 and the values of vertices are presented in Table 1. The system is in a steady state, and the working fluid is characterized by laminar flow, incompressibility, two-dimensionality and natural convection. The flow consists of nanofluids containing Fe_3O_4, TiO_2, and Cu particles, with water-EG serving as the base in a ternary nanofluid.

Table 1. Values of vertices.

Corner	Vertices
A (r_1, c_1)	(0.25, 0)
B (r_2, c_2)	(0.75, 0)
C (r_3, c_3)	(0.95, 0.35)
D (r_4, c_4)	(0.75, 0.75)
E (r_5, c_5)	(0.25, 0.75)
F (r_6, c_6)	(0.05, 0.35)

Additionally, a horizontal magnetic field is applied to the chamber for the purpose of this study. The cold surfaces (T_c) within the chamber are designed as square-shaped obstacles. The high temperature (T_h) is maintained at the base and bottom left walls of the hexagonal chamber, while the other walls are thermally insulated. The working model incorporates the Boussinesq approximation. This approximation assumes that density variations are insignificant except in buoyancy terms. This approach enables us to retain the fundamental principles of buoyancy-driven flow while enhancing the efficiency of numerical simulations, without significant compromise to accuracy. The domain experiences a gravitational force g acting downwards. Hexagonal cavities with square obstacles find applications across various fields by enhancing heat transfer, improving fluid mixing, optimizing acoustic properties, and creating advanced materials with novel properties. Their utility spans industries from thermal management and biomedical engineering to acoustics and materials science. The governing equations for this system are expressed below. The form of dimensional equations [3, 4] are:

Continuity:

$$\frac{\partial u}{\partial x}+\frac{\partial v}{\partial y}=0 \tag{1}$$

Momentum:

$$u\frac{\partial u}{\partial x}+v\frac{\partial u}{\partial y}+\frac{1}{\rho_{tnf}}\frac{\partial p}{\partial x}=\upsilon_{tnf}\left(\frac{\partial^2 u}{\partial x^2}+\frac{\partial^2 u}{\partial y^2}\right) \tag{2}$$

$$u\frac{\partial v}{\partial x}+v\frac{\partial v}{\partial y}+\frac{1}{\rho_{tnf}}\frac{\partial p}{\partial y}=\upsilon_{tnf}\left(\frac{\partial^2 v}{\partial x^2}+\frac{\partial^2 v}{\partial y^2}\right)+g\beta_{tnf}(T-T_0)-\frac{\sigma_{tnf}B_0^2}{\rho_{tnf}}v \tag{3}$$

Energy:

$$u\frac{\partial T}{\partial x}+v\frac{\partial T}{\partial y}=\alpha_{tnf}\left(\frac{\partial^2 T}{\partial x^2}+\frac{\partial^2 T}{\partial y^2}\right)+\lambda_1(T-T_0) \tag{4}$$

where, $\lambda_1=Q_0/(\rho c_p)_{tnf}$, and the nondimensional parameters are introduced as follows:

$$X=\frac{x}{L},\quad Y=\frac{y}{L},\quad U=\frac{uL}{\alpha_f},\quad V=\frac{vL}{\alpha_f},\quad P=\frac{pL^2}{\rho_{tnf}\alpha_f^2},\quad \theta=\frac{T-T_0}{\Delta T},\quad T_0=\frac{T_h+T_c}{2},\quad \Delta T=(T_h-T_c),\quad \Pr=\frac{\nu_f}{\alpha_f},\quad Ra=\frac{g\beta_f(T_h-T_c)L^3\Pr}{\nu_f\alpha_f},$$

$$Ha=B_0L\sqrt{\frac{\sigma_f}{\mu_f}},\quad Q=\frac{Q_0L^2}{k_f},\quad \alpha_f=\frac{k_f}{(\rho c_p)_f}$$

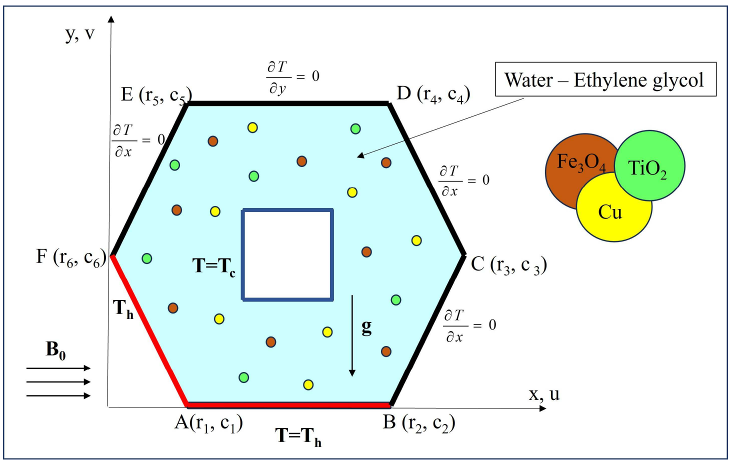

Fig. 1. Schematic of the considered geometry.

The non-dimensional forms of Eqs. (1) to (4) are:

$$\frac{\partial U}{\partial X}+\frac{\partial V}{\partial Y}=0 \tag{5}$$

$$U\frac{\partial U}{\partial X}+V\frac{\partial U}{\partial Y}=-\frac{\partial P}{\partial X}+S_1\left(\frac{\partial^2 U}{\partial X^2}+\frac{\partial^2 U}{\partial Y^2}\right) \tag{6}$$

$$U\frac{\partial V}{\partial X}+V\frac{\partial V}{\partial Y}=-\frac{\partial P}{\partial Y}+S_1\left(\frac{\partial^2 V}{\partial X^2}+\frac{\partial^2 V}{\partial Y^2}\right)+S_2-S_3 \tag{7}$$

$$U\frac{\partial \theta}{\partial X}+V\frac{\partial \theta}{\partial Y}=S_4\left(\frac{\partial^2 \theta}{\partial X^2}+\frac{\partial^2 \theta}{\partial Y^2}+Q\theta\right) \tag{8}$$

where $S_1=\Pr$, $S_2=Ra\Pr\theta$, $S_3=Ha^2\Pr V$ and $S_4=\alpha_{tnf}/\alpha_f$.

2.1. Boundary conditions

The specified boundary conditions are crucial for accurately simulating heat distribution within the hexagonal geometry. The constant hot temperature (T_h) on the base and left lower wall ensures a defined heat source, influencing convection and conduction within the boundary. Adiabatic conditions on the other walls prevent heat exchange through those surfaces, reflecting real-world scenarios where insulation or impermeable boundaries exist. The cold temperature (T_c) on the obstruction surface further defines heat extraction, impacting convective flows and temperature distributions. Together with no-slip conditions for fluid dynamics, these boundaries enable a comprehensive model of heat transfer phenomena, essential for practical and theoretical analysis. The following represent the boundary conditions of walls [17, 18]:

- For dimensional form

At AB wall	$u=v=0,$	$T=T_h=1$
At BC and CD wall	$u=v=0,$	$\partial T/\partial x=0$
At DE wall	$u=v=0,$	$\partial T/\partial y=0$
At EF wall	$u=v=0,$	$\partial T/\partial x=0$
At FA wall	$u=v=0,$	$T=T_h=1$
At obstacle	$u=v=0,$	$T=T_c=0.$

- For non-dimensional form

At AB wall	$U=V=0,$	$\theta=1$
At BC and CD wall	$U=V=0,$	$\partial\theta/\partial X=0$
At DE wall	$U=V=0,$	$\partial\theta/\partial Y=0$
At EF wall	$U=V=0,$	$\partial\theta/\partial X=0$
At FA wall	$U=V=0,$	$\theta=1$
At obstacle	$U=V=0,$	$\theta=0.$

2.2. Thermophysical characteristics

The ternary hybrid nanofluid is a composite fluid containing a base liquid with suspended nanoparticles of three different types. The performance of ternary hybrid nanofluid is dependent on the incorporation of three various types of nanoparticles into the base liquid. The combined effect of these nanoparticles often results in properties that are distinct from both the individual nanoparticle constituents and the base liquid. The presence of multiple nanoparticles can enhance stability through better dispersion mechanisms, especially with the use of surfactants or stabilizing agents. These enhanced properties make the ternary hybrid nanofluid an attractive option for various thermal management applications, offering a balance of improved thermal performance and stability. The volume accumulation coefficient, denoted as $\phi=\phi_1+\phi_2+\phi_3$, plays a significant role in determining the thermal characteristics of the tri-hybrid nanoliquid. The physical properties of ternary hybrid nanoliquids directly influence the enhancement of the working fluid's thermal features. It is essential to consider these properties as they greatly impact the overall performance. In Fig. 2, one can find the mathematical expressions that describe the thermophysical properties of teri-hybrid nanoliquid [5, 16]. Furthermore, thermal properties for correlations among tri-hybrid nanoparticles are provided, and their respective values can be found in Table 2 [7, 8].

Table 2. Thermophysical properties [7, 8].

Physical properties	Water-Ethylene glycol	Fe_3O_4	Cu	TiO_2
ρ	1056	5180	8933	4250
c_p	3288	670	85	686.2
k	0.425	9.7	401	8.9538
β	0.00341×10^{-5}	1.3×10^{-5}	1.67×10^{-6}	0.9×10^{-6}
σ	0.00509	0.74×10^{6}	59.6×10^{6}	2.6×10^{6}
Pr	29.86	-	-	-

Table 3. Detailed information on the optimum mesh type.

Mesh selection	Extremely fine
Number of elements	32592
Nodes	17551
Number of Triangles	30924
Number of Quads	1668
Edge of elements	842

3. Solution Procedure

The current investigation involves conducting simulations by solving Eq. (1) to (4) and applying the boundary conditions. This is achieved using the Academic Institutional Licensed software "COMSOL Multiphysics 6.1". The FEM method is applied to solving Eq. (5) to (8) in conjunction with the nondimensional boundary conditions. To improve the precision of the parametric study, additional refined meshes are employed to handle all boundary layers. At the outset, the computational domain is divided into a non-uniform triangular mesh comprising various element sizes. Subsequently, the primary equations are converted into sets of nonlinear algebraic equations. Through the application of essential boundary conditions (BC), the element matrices are integrated into global matrices. The solution method is iteratively executed until the convergence criteria are met.

To facilitate computation, the domain is initially divided into a finite number of asymmetrical triangular mesh elements. The discretization principle guarantees fast convergence and reliability of the method. The meshing configuration for the current problem is depicted in Fig. 3 and the detailed information on the optimum mesh type are presented in Table 3. By imposing the appropriate BC, the element matrices are transformed into global matrices. The flow chart of modeling steps using in this study is depicted in Fig. 4.

3.1. Validation

The existing research on FEM with COMSOL software has been comprehensively confirmed and supported by validating Fig. 5 through comparison with Islam et al. [22] regarding natural convection in an octagonal enclosure at $Ra = 10^4$ and $Pr = 0.71$. Figure 5 showcases the contour plots of streamlines and isotherms, which have been meticulously compared with the corresponding results from Islam et al. [22]. This comparison reveals a high degree of similarity, indicating that the numerical model accurately captures the convection patterns and temperature distributions within the enclosure. The alignment of these plots provides strong evidence of the model's validity, demonstrating its capability to replicate established results reliably.

$$\mu_{nf} = \frac{\mu_{bf}}{(1-\phi)^{2.5}}$$
$$\rho_{nf} = \phi\rho_1 + (1-\phi)\rho_{bf}$$
$$(\rho\beta)_{nf} = \phi(\rho\beta)_1 + (1-\phi)(\rho\beta)_{bf}$$
$$(\rho C_p)_{nf} = \phi(\rho C_p)_{bf} + (1-\phi)(\rho C_p)_{bf}$$
$$\alpha_{nf} = \frac{k_{nf}}{(\rho C_p)_{nf}}$$
$$\frac{k_{nf}}{k_{bf}} = \left(\frac{k_3 + 2k_f - 2\phi_3(k_{bf} - k_3)}{k_3 + 2k_f + \phi_3(k_{bf} - k_3)}\right)$$
$$\frac{\sigma_{nf}}{\sigma_{bf}} = \frac{(1+2\phi_3)\sigma_3 + (1-2\phi_3)\sigma_{bf}}{(1-\phi_3)\sigma_3 + (1+\phi_3)\sigma_{bf}}$$

(a)

$$\mu_{hnf} = \frac{\mu_{bf}}{(1-\phi_1-\phi_2)^{2.5}}$$
$$\rho_{hnf} = (1-\phi)\rho_{bf} + \phi_1\rho_1 + \phi_2\rho_2$$
$$(\rho\beta)_{hnf} = \phi_1(\rho\beta)_1 + \phi_2(\rho\beta)_2 + (1-\phi)(\rho\beta)_{bf}$$
$$(\rho C_p)_{hnf} = \phi_1(\rho C_p)_1 + \phi_2(\rho C_p)_2 + (1-\phi)(\rho C_p)_{bf}$$
$$\alpha_{hnf} = \frac{k_{hnf}}{(\rho C_p)_{hnf}}$$
$$\frac{k_{hnf}}{k_{nf}} = \left(\frac{k_2 + 2k_{nf} - 2\phi_2(k_{nf} - k_2)}{k_2 + 2k_{nf} + \phi_2(k_{nf} - k_2)}\right)$$
$$\frac{\sigma_{hnf}}{\sigma_{nf}} = \frac{(1+2\phi_2)\sigma_2 + (1-2\phi_2)\sigma_{nf}}{(1-\phi_2)\sigma_2 + (1+\phi_2)\sigma_{nf}}$$

(b)

$$\mu_{tnf} = \frac{\mu_{bf}}{(1-\phi_1-\phi_2-\phi_3)^{2.5}}$$
$$\frac{\rho_{tnf}}{\rho_{bf}} = (1-\phi_1)\left[(1-\phi_2)\left\{(1-\phi_3) + \phi_3\frac{\rho_3}{\rho_{bf}}\right\} + \phi_2\frac{\rho_2}{\rho_{bf}}\right] + \phi_1\frac{\rho_1}{\rho_{bf}}$$
$$(\rho\beta)_{tnf} = (1-\phi_1-\phi_2-\phi_3)(\rho\beta)_{bf} + (\rho\beta)_1\phi_1 + (\rho\beta)_2\phi_2 + (\rho\beta)_3\phi_3$$
$$\frac{(\rho cp)_{tnf}}{(\rho cp)_{bf}} = (1-\phi_1)\left[(1-\phi_2)\left\{(1-\phi_3) + \phi_3\frac{(\rho cp)_3}{(\rho cp)_{bf}}\right\} + \phi_2\frac{(\rho cp)_2}{(\rho cp)_{bf}}\right] + \phi_1\frac{(\rho cp)_1}{(\rho cp)_{bf}}$$
$$\alpha_{tnf} = \frac{k_{tnf}}{(\rho C_p)_{tnf}} \qquad \frac{\sigma_{tnf}}{\sigma_{hnf}} = \frac{(1+2\phi_1)\sigma_1 + (1-2\phi_1)\sigma_{hnf}}{(1-\phi_1)\sigma_1 + (1+\phi_1)\sigma_{hnf}}$$
$$\frac{k_{tnf}}{k_{hnf}} = \left(\frac{k_1 + 2k_{hnf} - 2\phi_1(k_{hnf} - k_1)}{k_1 + 2k_{hnf} + \phi_1(k_{hnf} - k_1)}\right)$$

(c)

Fig. 2. The mathematical expressions describing the thermophysical properties of teri-hybrid nanoliquid, (a) Nanofluid, (b) Hybrid nanofluid, (c) Ternary hybrid nanofluid

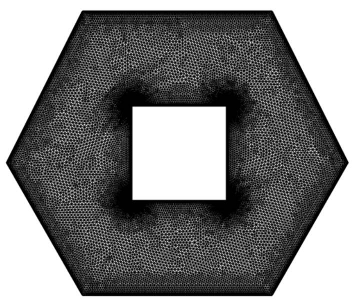

Fig. 3. Computational grid chosen after mesh.

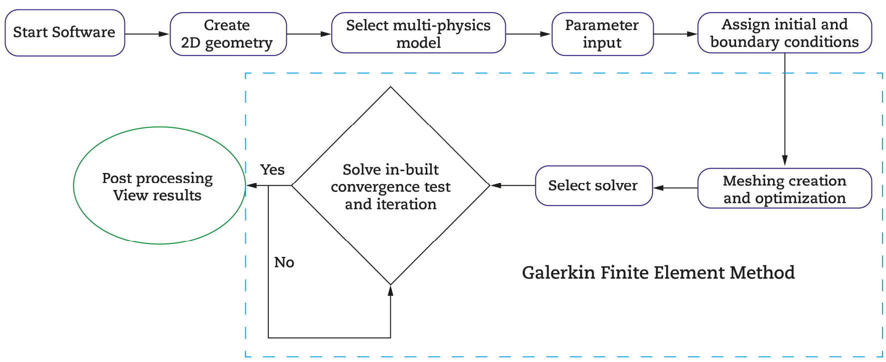

Fig. 4. The flow chart of modelling steps used in this study.

Table 4. Comparison for various *Ra* when *Pr* = 0.7

Ra	De Vahl davis [25]	Sheikholeslami et al. [24]	Present
10^3	1.118	1.1432	1.1183
10^4	2.243	2.2749	2.2431
10^5	4.519	4.5199	4.5197

Furthermore, the quantitative validation is reinforced by Table 4, which compares key numerical values obtained from the simulations with those reported by Islam et al., The close agreement between these values underscores the accuracy of the model. Such consistency instills confidence in the reliability of the obtained results, affirming that the model can be trusted for further investigations. The successful validation against a recognized study paves the way for the exploration of more complex scenarios and the extension of the model to different geometries and conditions. This rigorous validation process not only confirms the robustness of the FEM approach with COMSOL software but also highlights its potential for advancing research in natural convection and related phenomena. By building on this validated framework, future studies can delve deeper into the nuances of convection processes, contributing to the broader understanding and application of thermal management strategies.

4. Graphical Output and Discussion

In the current simulation, attention is placed on studying the constant, smooth, magnetohydrodynamic motions of the tri-hybrid Fe_3O_4–Cu-TiO_2-Kerosene nanoparticles within a hexagonal chamber that contains a cold square obstacle. The boundary conditions of the primary Eqs. (5) to (8) have been analyzed using the FEM. The computational parameters for this study are set as follows: Hartmann number ($0 \le Ha \le 90$), Rayleigh number ($10^3 \le Ra \le 10^5$) and Heat generation and sink ($-5 \le Q \le 15$).

4.1. Consequence of *Ra*

Figure 6 illustrates the alteration in streamlines and isotherms due to variations in *Ra* while keeping *Pr* constant at 29.86, ϕ at 0.05, *Ha* at 90 and Q at 2. It can be observed that the velocity profile in Fig. 6 exhibits a symmetrical distribution inside the hexagonal chamber. As the flow is induced, it initiates the development of an internal eddy which commences at the lower part of the obstruction. The elevated temperatures at the base and lower-left section of the chamber wall contribute to an intensification in the inner vortex movement near the obstacle. The flow lines within the internal vortex experiences an augmentation. In the case of $Ra = 10^5$, the eddy extends from the lower wall of the obstruction to the cold wall on the left side, resulting in an elongated vortex. With the increase in *Ra*, the circulation and convection of the fluid flow intensifies. The convective motion causes the fluid to move in a circular pattern near the heated walls, with the density of the fluid being lower in this region. As the less dense fluid enters the cooler zone, the sturdiness of the motion decreases. When the value of *Ra* is increased, the buoyancy-driven convection intensifies.

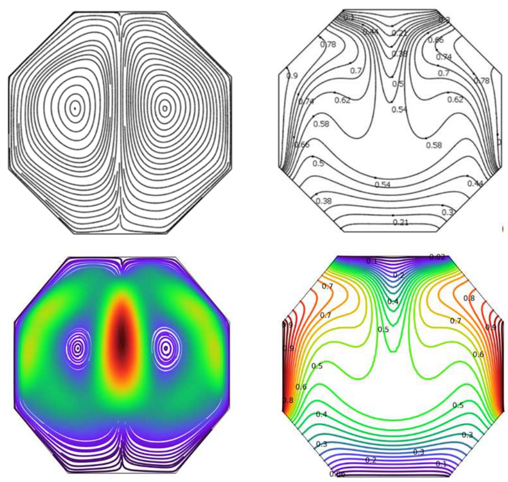

Fig. 5. Comparison of contours plots for streamlines and isotherms for thermal Rayleigh number value $Ra = 10^4$ and Prandtl number value $Pr = 0.71$ for present method (FEM) and Islam et al. [22] (Row 1).

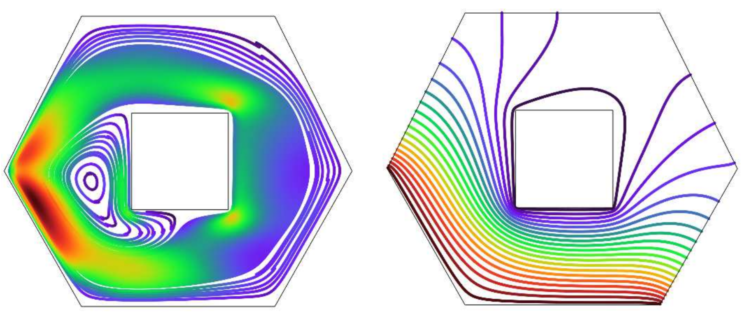

(a)

Fig. 6. Streamline and Isotherm contours for $Pr = 29.86$, $\phi = 0.05$, $Ha = 90$, Q = 2 with various *Ra* values, (a) $Ra = 10^3$, (b) $Ra = 10^4$, (c) $Ra = 10^5$.

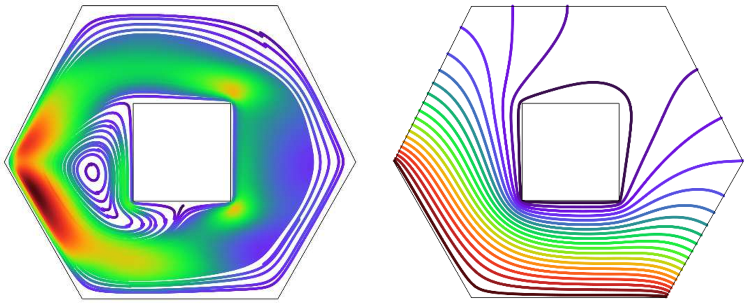

(b)

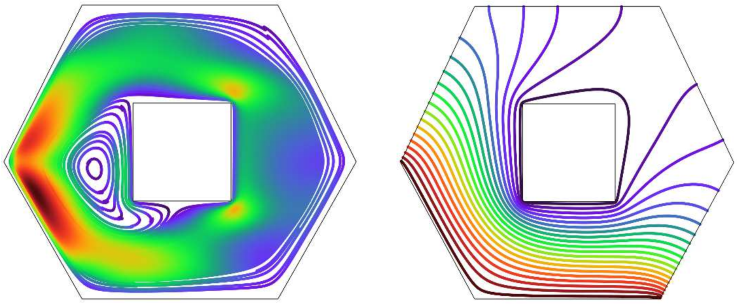

(c)

Fig. 6. Continued.

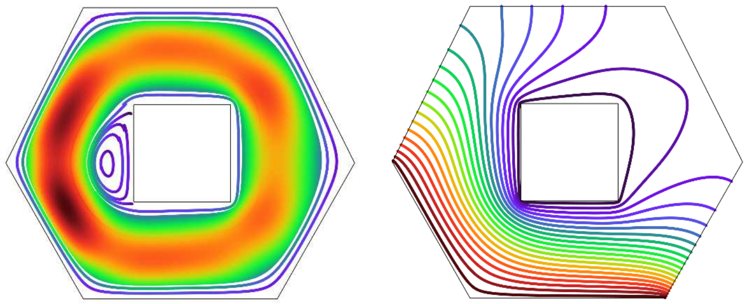

(a)

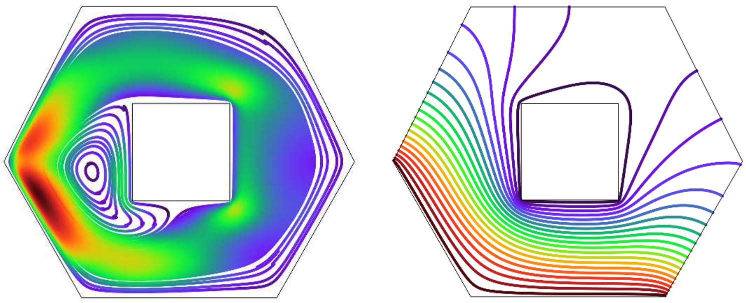

(b)

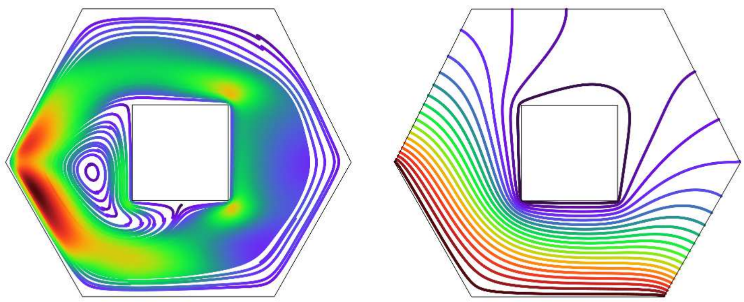

(c)

Fig. 7. Streamline and Isotherm contour for Pr = 29.86, ϕ = 0.05, Ra = 10^4, Q = 2 with various Ha values, (a) Ha = 0, (b) Ha = 70, (c) Ha = 90.

The temperature distribution contour reveals the upward movement of liquid within the outer enclosure. The heat is transmitted near the top of the right side of the outer boundary as a result of the fluid's circulation within the block. Examining the temperature contour, we observe that the isotherms are in closer proximity to the bottom and left side walls of the cold obstacle. The flow movement from the upper and right sides of the outer boundary is relatively weak. Initially, the heat distribution rises upwards when the fluid passes through the obstacle and then descends. The temperature of the fluid near the wall section of the block is higher than that of the fluid near the colder walls. The fluid ascends from the heated wall of the hexagonal chamber due to heat convection. When *Ra* increases, the temperature also enhances, resulting in an increased strength of temperature distribution.

4.2. Consequence of *Ha*

Figure 7 showcases the changes in streamlines and isotherms caused by various values of *Ha* while maintaining a constant value for $Pr = 29.86$, $\phi = 0.05$, $Ra = 10^4$ and Q = 2. The presence of a magnetic field induces the Lorentz force, which significantly affects the flow behavior of the electrically conducting fluid within the chamber. Even in the devoid situation of *Ha*, the tri-hybrid nanofluid within the chamber creates a smooth circulation, and streamlines depict typical convective rolls and circulations driven by buoyancy forces. The effect of the Lorentz force is minimal, and the fluid retains its natural convective patterns, characterized by strong recirculation zones and high velocity gradients. This internal eddy strengthens as $Ha = 70$ increases near the left wall of the cold region. The velocity decreases significantly in the presence of a strong magnetic field. The magnetic effect in the motion regime generates the Lorentz force, which, in turn, hinders the convection current. The retarding effect of the magnetic field causes a backward motion in the streamlines. The enhancement of $Ha = 90$ forms a weak innermost eddy moving along the bottom wall of the square obstacle. The Lorentz force becomes more pronounced, flattening the velocity profiles and reducing the peak velocities. This results in more uniform and stable flow patterns, with less pronounced velocity gradients. The Lorentz forces are developed as the magnetic field increases, resulting in a reduction in velocity. With increasing magnetic field strength, the streamlines become more aligned with the direction of the magnetic field. The convective rolls are suppressed, leading to more straightened and less chaotic streamline patterns. The circulation patterns become more orderly and aligned with the magnetic field lines, indicating a transition towards conduction-dominated heat transfer. The velocity field declines as *Ha* increases. However, the velocity has been completely suppressed when the magnetic field strength is high.

The vigorous circulation and strong convective currents at low *Ha* enhance the heat transfer rate. The continuous movement of fluid between the hot and cold surfaces maximizes the thermal gradient and the overall heat exchange efficiency. At higher *Ha* values, the convective currents are significantly suppressed, and the heat transfer mechanism is dominated by conduction. The heat exchange becomes less efficient as the fluid movement is minimized, and thermal energy transfer relies solely on molecular diffusion, which is inherently slower.

The isotherms depicted in the figure illustrate how transmission of heat has an effect in the devoid situation ($Ha = 0$) of a magnetic field. Moreover, the transmission of heat is minimized when a higher ($Ha = 70$) Lorentz effect is present. As the magnetic field strength increases ($Ha = 90$), the sturdiness of the temperature lines decreases. The buoyancy-driven mechanism has also reduced due to the influence of Lorentz forces. The heat has been transported from the hot wall on the bottom and left side of the outer boundary through the tri-hybrid nanofluid movement within the compartment, and it descends along the cold wall. Consequently, the exchange of energy decreases as the density of isotherms decreases. An increase in *Ha* results in a decrease in the transportation of heat, ultimately leading to a reduction in thermal within the block.

4.3. Consequence of heat source and sink

The streamline contour represents in Fig. 8 various Q values with stable values of $Ra = 10^4$ and *Ha* value of 70. The diagram shows the influences of heat absorption or source (Q) on the flow patterns of Fe_3O_4-Cu-TiO_2 with Water-Ethylene glycol based ternary hybrid nanofluid. A less pronounced circulation cell is formed along the bottom left wall of the square obstacle within the main vortex when the heat sink value is set to Q = -5. As a result, the exchange of heat decreases at the hot wall, indicating the dominance of conduction. Without any heat input (Q = 0), the internal vortex moves towards the upper part of the cold wall on the left side. The convective mode is more noticeable and the flow pattern becomes stronger. However, as the heat input Q increases, the flow intensity diminishes near the right side of the outer boundary. In the case of Q = 15, the primary and its inner circulation cells elongate along the hot walls and contract near the adiabatic walls due to higher flow velocity. Furthermore, when the heat source coefficient increases, the impact of convective heat transfer becomes more significant.

The isotherm contour is shown in Fig. 8 for various Q values with stable values of $Ra = 10^5$ and *Ha* value of 90. The flow of heat near the hot wall in the hexagonal chamber is smooth, while it moves towards the top adiabatic wall. The hot walls of the chamber exhibit a stronger fluid flow, whereas the cold region of the compartment experiences a weaker flow. The temperature is significantly decreased around the colder wall due to the presence of cold. In the absence of heat (Q = 0), the movement of heat intensifies along the left side and bottom wall of the outer boundary but diminishes in the obstacle region. The increase in the value of Q leads to higher temperature lines along the bottom and left wall of the domain. The presence of a pronounced circulation pattern around the colder obstacle is observed when Q is increased at a value of 15. Additionally, an enhancement in the value of Q results in an enhanced flow of heat within the outer boundary. The decline in heat exchange at the hot wall is indicative of a conduction-dominated regime under heat sink conditions, while the increased heat source coefficient emphasizes the significance of convective heat transfer. Both phenomena illustrate the dynamic interplay between conduction and convection in the system, necessitating a balanced approach to optimize thermal management. The observed temperature patterns provide valuable insights into the thermal management and energy transfer efficiency within the system. Effective thermal management is characterized by uniform temperature distribution and minimal gradients, while changes in heat input can significantly influence the system’s efficiency and performance. Optimal heat input levels are crucial for maintaining balanced energy transfer, ensuring the longevity and reliability of the thermal energy storage system.

4.4. The Nusselt number

The computation for the local *Nu* value pertaining to the heated bottom wall has been carried out. The equation encompassing the local *Nu* is presented below, wherein a dimensionless temperature is employed:

$$Nu = -\frac{k_{tnf}}{k_f}\left(\frac{\partial \theta}{\partial Y}\right)_{X=0} \tag{9}$$

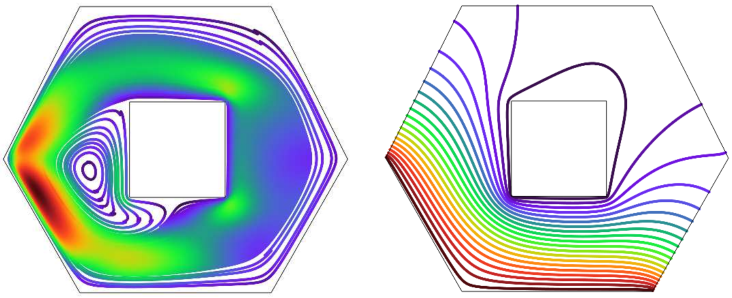

(a)

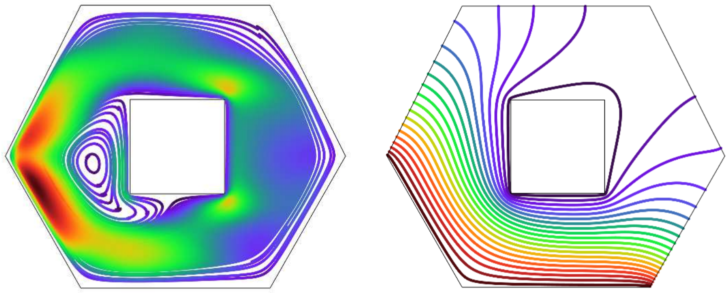

(b)

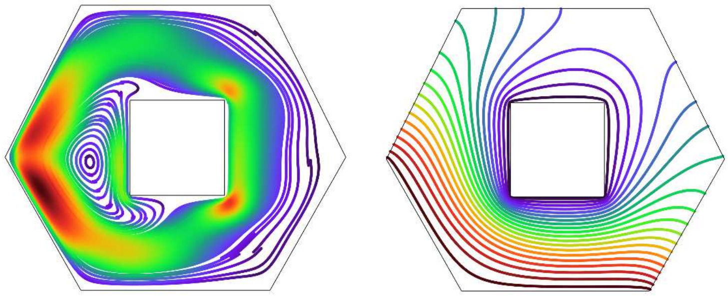

(c)

Fig. 8. Streamline and Isotherm contour for Pr = 29.86, ϕ = 0.05, Ra = 10^4, Ha = 70 with various Q values, (a) Q = -5, (b) Q = 0, (c) Q = 15.

4.5. Thermal distribution

Figure 9 presents a graphical representation of the local heat transfer rate with Ra along the bottom wall of the enclosure for Fe_3O_4-Cu-TiO_2 nanofluid. The temperature profile indicates that the increase in Ra leads to an enhancement in Nu. This occurrence can be attributed to the rise in flow velocity as Ra increases. At low Rayleigh numbers, the heat transfer within the enclosure is primarily dominated by conduction. The buoyancy forces are weak compared to the viscous forces, leading to minimal fluid motion. The temperature profile along the bottom wall begins to show non-linear characteristics, with regions of steep temperature gradients corresponding to the formation of convective cells. The local heat transfer rate increases, particularly in areas where convective updrafts and downdrafts enhance the thermal mixing. When Ra remains constant, the exchange of energy intensifies as the fluid ascends within the chamber. However, as the liquid moves along the cold wall, the heat transmission rate diminishes due to the thermal reduction in the middle section of the cavity. As a result, there is a decrease in temperature distribution. This drop can be traced back to the heat loss of the fluid between the cold wall and the outer boundary wall, which leads to a decline in heat exchange. Consequently, the heat transmission rate increases, leading to a general augmentation in the local Nu near the adiabatic of the block. This effect becomes more pronounced with higher Ra values and temperature distribution. The temperature distribution along the bottom wall shows pronounced fluctuations, corresponding to the presence of convective rolls or cells. The local heat transfer rate is significantly higher, especially in regions where fluid motion enhances thermal exchange between the hot wall and the bulk fluid. These convective currents create hot and cold spots along the wall, resulting in a highly non-linear temperature profile.

Figure 10 illustrates the local Nu profiles under different magnetic field strengths. The curves exhibit a rising pattern for low magnetic parameters. Conversely, a contrasting trend is observed for higher values of the Hartmann number. The local Nu profiles increase with decreasing values of Ha, while they decrease when the magnetic field strength is enhanced. In increasing Ha, which corresponds to a stronger magnetic field, results in a significant reduction in fluid velocities and a suppression of convective circulation patterns. This transition from convection-dominated to conduction-dominated heat transfer highlights the critical role of the magnetic field in modulating the fluid motion and thermal performance within the chamber.

Figure 11 depicts the local Nu distribution with heat generation and sink along the bottom wall of the chamber for teri-hybrid nanofluid. The observed decline in heat exchange at the hot wall indeed suggests a shift towards conduction-dominated heat transfer under the conditions of the heat sink. This can be attributed to the reduced temperature gradient and the diminished influence of convective mechanisms. The heat sink conditions likely promote a more uniform temperature distribution, thereby minimizing the convective currents and emphasizing conductive heat transfer. Nu increases when the heat source is magnified, while the local heat transfer rate decreases with increasing heat sink/absorption. This leads to an overall enhancement in the Nu distribution.

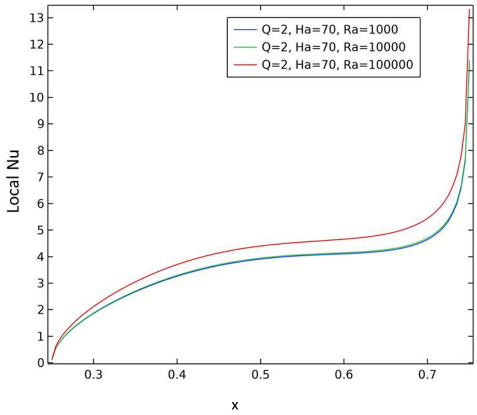

Fig. 9. Local *Nu* for Q = 2, *Pr* = 29.86, ϕ = 0.05, *Ha* = 70 with various *Ra* value at bottom heated wall.

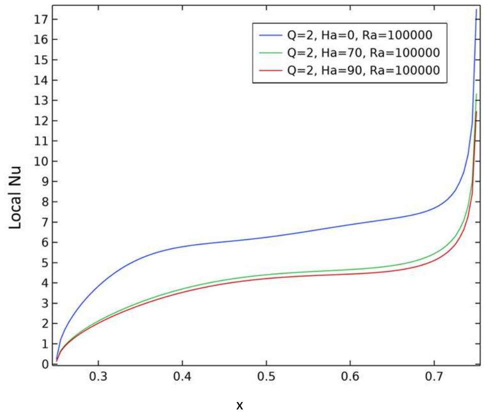

Fig. 10. Local *Nu* for Q = 2, *Pr* = 29.86, ϕ = 0.05, *Ra* = 10^5 with various *Ha* value at bottom heated wall.

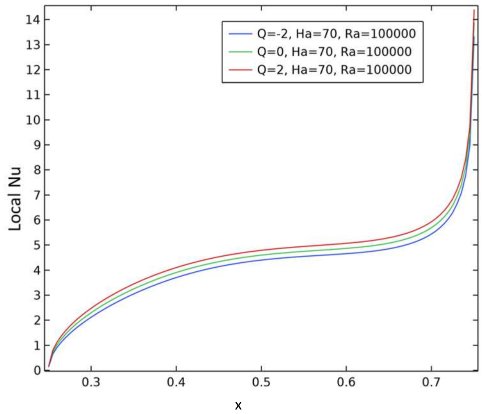

Fig. 11. Local *Nu* for *Ha* = 70, *Pr* = 29.86, ϕ = 0.05, *Ra* = 10^5 with various Q value at bottom heated wall.

Conversely, the opposite effect is observed for heat sink, resulting in a decrease in the *Nu* due to a decrease in the temperatures of the internal nanofluid. The increase in the heat source coefficient underscores the critical role of convective heat transfer in the system. As the coefficient increases, it enhances the heat transfer rate from the heat source to the surrounding medium, thereby amplifying the convective effects. This highlights the importance of optimizing the convective heat transfer mechanisms to improve overall thermal performance. It is worth noting that the local heat transfer rate profiles exhibit an upward shape in all three cases.

5. Conclusion

The present study utilized nanofluids consisting of Fe_3O_4, Cu and TiO_2 particles in a water-ethylene glycol base. These nanofluids were used in a ternary nanofluid system within a hexagonal chamber containing a square obstacle. Eqs. (5) to (8) were used in the FEM implementation in the “COMSOL Multiphysics 6.1” commercial software. The use of tri-hybrid nanofluids in the flow problems resulted in a significant enhancement in the transportation of heat performance. The cold surfaces within the chamber were designed as square-shaped obstacles. The high temperature was maintained at the base and bottom left walls of the hexagonal chamber, while the other walls were thermally insulated. Additionally, a horizontal magnetic field was applied within the chamber. The simulations were conducted for a range of *Ra* from 10^3 to 10^5. The variations in the heat source and absorption term (Q) from -5 to 15 were utilized. *Ha* was set at 0, 70 and 90. The Prandtl number (*Pr*) determined for the ethylene glycol was found to be 29.86. The use of tri-hybrid nanoliquids in the flow problems resulted in a significant enhancement in the transportation of heat performance.

The main outcomes from the simulations are summarized below:

For the variation of *Ra*:

- As *Ra* increases, the fluid flow experiences greater circulation and convection. This convection leads to a circular movement of the liquid near the heated walls. When *Ra* is elevated, the buoyancy-driven convection intensifies.
- The fluid in the vicinity of the hot wall section of the block exhibits a higher temperature compared to the fluid near the colder walls. Heat convection causes the fluid to rise from the heated wall of the hexagonal cavity. With an increase in Ra, the temperature also rises, resulting in a stronger temperature distribution.
- The rate of transmission of heat increases, leading to an overall enhancement in the local *Nu* near the adiabatic of the block. This effect becomes more pronounced as *Ra* values and temperature distribution rise.

For the variation of *Ha*:

- There is a significant decrease in velocity when there is a strong magnetic field present. This magnetic effect on the motion produces the Lorentz force. With increasing *Ha*, the velocity field experiences a decrease. At high magnetic field strengths, the velocity is completely suppressed.

- Furthermore, with an increase in magnetic field strength, the sturdiness of the temperature lines diminishes. The movement of heat within the compartment, facilitated by the tri-hybrid nanofluid, transports heat from the hot wall on the bottom and left side of the outer boundary. As the density of isotherms decreases, the exchange of energy decreases as well. Consequently, an increase in *Ha* causes a reduction in heat transportation, ultimately leading to a decrease in temperature within the block.
- The *Nu* profiles in the vicinity rise as *Ha* values decrease, whereas they decline with an increase in the strength of the magnetic field.

The noticed alterations in heat generation and absorption:

- The decline in heat exchange at the hot wall indicates that conduction prevails in terms of heat sink value. As the heat source coefficient increases, the significance of convective heat transfer becomes more apparent.
- An observable circulation pattern is present around the colder obstacle as Q is increased, the temperature lines along the hot wall of the domain become higher with the increase in Q.
- The *Nu* (Nusselt number) experiences an increase as the heat source is amplified, while the local heat transfer rate diminishes with a rise in heat sink/absorption. It is important to note that the local heat transfer rate profiles exhibit an upward shape across all three values.

In microfluidics, hexagonal cavities with square obstacles are used in lab-on-a-chip devices. These devices are crucial in biomedical applications for processes such as cell sorting, chemical reactions, and diagnostics. The specific geometry can facilitate the mixing of fluids at microscale levels, ensuring uniform distribution of reagents and enhancing reaction kinetics. Architectural acoustics also benefit from such configurations. The design of concert halls and auditoriums can incorporate hexagonal cavities with obstacles to improve sound diffusion and reduce echo, ensuring better sound quality. This application leverages the ability of the cavity and obstacle geometry to scatter sound waves effectively.

Future studies could focus on experimental validation of these proposed improvements using advanced measurement techniques to accurately assess thermal performance under realistic operating conditions. Exploring the use of different materials or coatings for the obstruction could alter its thermal conductivity and interaction with the nanofluid, potentially improving thermal management and efficiency. Surface modification of nanoparticles could enhance their dispersion and stability within the base fluid, thereby improving overall thermal performance and longevity of the nanofluid. Furthermore, exploring the broader implications of the findings for practical applications holds promise for future endeavors. This discovery has the potential to be valuable in various engineering and industrial sectors for enhancing thermal efficiency.

Nomenclature

Ha	Hartmann number	Q_0	Dimensional heat source
Pr	Prandtl number	Ra	Rayleigh number
u	Dimensional velocity component with respect to x direction	C_p	Specific heat of fluid [J.kg^{-1}.K^{-1}]
B_0	Strength of magnetic field	p	Pressure [N/m^2]
x, y	Cartesian coordinate [m]	T	Temperature [K]
L	Length of the cavity [m]	X, Y	Non-dimensional coordinate [m/s]
U	Dimensionless velocity	Q	Heat generation
v	Dimensional component with respect to y direction [m/s]	T_c	Temperature at cold wall
T_h	Temperature at hot wall	g	Gravity acceleration
Nu	Local Nusselt number	V	Dimensionless velocity
		k	Thermal conductivity [W/mK]

Symbol	**Greek Letters**		
α	Thermal Diffusivity [m^2/s]	ν	Kinematic viscosity [m^2/s]
ϕ	Volume fraction	ρ	Fluid density [kg/m^3]
θ	Non dimensional temperature	σ	Electrical conductivity [S/m]
μ	Dynamic viscosity [Pa.s]	β	Thermal expansion coefficient [1/K]

Symbol	**Subscript**
nf	Nanofluid
tnf	Ternary nanofluid
f	Base fluid
hnf	Hybrid nanofluid

Author Contributions

A. Thilagavthi developed the numerical model, conducted the simulations, wrote the manuscript and prepared all the figures under the guidance of V. Ramachandra Prasad. The manuscript was written through the contribution of all authors. All authors discussed the results, reviewed, and approved the final version of the manuscript.

Acknowledgments

Not Applicable.

Conflict of Interest

The authors declared that they don't have any conflict of interest.

Funding

No funding was received for conducting this study.

Data Availability Statements

The datasets generated during the current study are available from the corresponding author on reasonable request.

Reference

[1] Eftekhari, S.A., Hekmatifar, M., Toghraie, D., Esfe, M.H., A feed-forward artificial neural network with several training methods and various geometries for predicting the rheological behavior of Al_2O_3/ethylene glycol-water hybrid nanofluid, *Ain Shams Engineering Journal*, 14(11), 2023, 102555.

[2] Afzal, S., Qayyum, M., Akgül, A., Hassan, A.M., Heat transfer enhancement in engine oil based hybrid nanofluid through combustive engines: An entropy optimization approach, *Case Studies in Thermal Engineering*, 52, 2023, 103803.

[3] Javed, T., Mehmood, Z., Pop, I., MHD-mixed convection flow in a lid-driven trapezoidal cavity under uniformly/non-uniformly heated bottom wall, *International Journal of Numerical Methods for Heat and Fluid Flow*, 27(6), 2017, 1231-1248.

[4] Teamah, M.A., El-Maghlany, W.M., Augmentation of natural convective heat transfer in square cavity by utilizing nanofluids in the presence of magnetic field and uniform heat generation/absorption, *International Journal of Thermal Sciences*, 58, 2012, 130-142.

[5] Mansour, M.A., Siddiqa, S., Gorla, R.S.R., Rashad, A.M., Effects of heat source and sink on entropy generation and MHD natural convection of Al_2O_3-Cu/water hybrid nanofluid filled with square porous cavity, *Thermal Science and Engineering Progress*, 6, 2018, 57-71.

[6] Nisar, K.S., Khan, U., Zaib, A., Khan, I., Baleanu, D., Numerical simulation of mixed convection squeezing flow of a hybrid nanofluid containing magnetized ferroparticles in 50%: 50% of ethylene glycol–water mixture base fluids between two disks with the presence of a non-linear thermal radiation heat flux, *Frontiers in Chemistry*, 8, 2020, 792.

[7] Saranya, S., Baranyi, L., Al-Mdallal, Q.M., Free convection flow of hybrid ferrofluid past a heated spinning cone, *Thermal Science and Engineering Progress*, 32, 2022, 101335.

[8] Das, S., Mahato, N., Ali, A., Jana, R.N., Dynamical behaviour of magneto-copper-titania/water-ethylene glycol stream inside a gyrating channel, *Chemical Physics Letters*, 793, 2022, 139476.

[9] Bejan, A., Khair, K.R., Heat and mass transfer by natural convection in a porous medium, *International Journal of Heat and Mass Transfer*, 28, 1985, 909-918.

[10] Yuan, X., Tavakkoli, F., Vafai, K., *Analysis of natural convection in horizontal concentric annuli of varying inner shape*, Taylor & Francis, 2015.

[11] Oztop, H.F., Abu-Nada, E., Numerical study of natural convection in partially heated rectangular enclosures filled with nanofluids, *International Journal of Heat and Fluid Flow*, 29(5), 2008, 1326-1336.

[12] Haq, R.U., Soomro, F.A., Mekkaoui, T., Al-Mdallal, Q.M., MHD natural convection flow enclosure in a corrugated cavity filled with a porous medium, *International Journal of Heat and Mass Transfer*, 121, 2018, 1168-1178.

[13] Anandalakshmi, R., Kaluri, R.S., Basak, T., Heatline based thermal management for natural convection within right-angled porous triangular enclosures with various thermal conditions of walls, *Energy*, 36, 2011, 4879- 4896.

[14] Sheikhzadeh, G.A., Arefmanesh, A., Kheirkhah, M.H., Abdollahi, R., Natural convection of Cu–water nanofluid in a cavity with partially active side walls, *European Journal of Mechanics-B/Fluids*, 30, 2011, 166-176.

[15] Zahan, I., Nasrin, R., Khatun, S., Thermal performance of ternary-hybrid nanofluids through a convergent-divergent nozzle using distilled water-ethylene glycol mixtures, *International Communications in Heat and Mass Transfer*, 137, 2022, 106254.

[16] Ullah, A.Z., Guo, X., Gul, T., Ali, I., Saeed, A., Galal, A.M., Thin film flow of the ternary hybrid nanofluid over a rotating disk under the influence of magnetic field due to nonlinear convection, *Journal of Magnetism and Magnetic Materials*, 573, 2023, 170673.

[17] Nadeem, S., Akber, R., Ghazwani, H.A., Alzabut, J., Hassan, A.M., Numerical computations for convective MHD flow of viscous fluid inside the hexagonal cavity having sinusoidal heated walls, *Results in Physics*, 56, 2024, 107229.

[18] Thirumalaisamy, K., Sivaraj, R., Reddy, A.S., Fluid flow and heat transfer analysis of a ternary aqueous Fe3O4+ MWCNT+ Cu/H2O magnetic nanofluid in an inclined rectangular porous cavity, *Journal of Magnetism and Magnetic Materials*, 589, 2024, 171503.

[19] Thirumalaisamy, K., Reddy, A.S., Numerical computation on MHD natural convective ternary nanofluid flow and heat transfer in a porous square cavity: Marker-and-cell technique, *International Journal of Numerical Methods for Heat and Fluid Flow*, 33(10), 2023, 3425-3466.

[20] Vinodhini, N., Prasad, V.R., Numerical study of magneto convective Buongiorno nanofluid flow in a rectangular enclosure under oblique magnetic field with heat generation/absorption and complex wall conditions, *Heliyon*, 9(7), 2023, e17669.

[21] Vinodhini, N., Prasad, V.R., Numerical study of free convection ag-water nanofluid flow in a square enclosure with viscous dissipation and heat generation/ absorption effects in a porous medium with complex wall conditions, *Journal of Porous Media*, 26(9), 2023, 77-99.

[22] Islam, Q., Hasan, M.N., Saha, S., Saha, G., Natural convection heat transfer within octagonal enclosure, *International Journal of Engineering*, 23, 2010, 1-10.

[23] Vinodhini, N., Prasad, V.R., Magneto-hybrid nanofluid (Al2O3/Cu-Oil) flow in a porous square enclosure with Cattaneo-Christov heat flow model-sensitivity analysis, *Indian Journal of Chemical Technology*, 30(5), 2023, 714-730.

[24] Sheikholeslami, M., Vajravelu, K., Rashidi, M.M., Forced convection heat transfer in a semi annulus under the influence of a variable magnetic field, *International Journal of Heat and Mass Transfer*, 92, 2016, 339-348.

[25] de Vahl Davis, G., Natural convection of air in a square cavity: a bench mark numerical solution, *International Journal for Numerical Methods in Fluids*, 3(3), 1983, 249-264.

[26] Khademi, A., Abtahi Mehrjardi, S.A., Said, Z., Chamkha, A.J., Heat Transfer Improvement in a Thermal Energy Storage System using Auxiliary Fluid Instead of Nano-PCM in an Inclined Enclosure: A Comparative Study, *Journal of Applied and Computational Mechanics*, 9(2), 2023, 475-486.

[27] Mehrjardi, S.A.A., Khademi, A., Said, Z., Ushak, S., Chamkha, A.J., Enhancing latent heat storage systems: the impact of PCM volumetric ratios on energy storage rates with auxiliary fluid assistance, *Energy Nexus*, 11, 2023, 100227.

[28] Khademi, A., Darbandi, M., Schneider, G.E., Numerical study to optimize the melting process of phase change material coupled with extra fluid, *In AIAA Scitech 2020 Forum*, 2020.

[29] Khademi, A., Mehrjardi, S.A., Tiari, S., Mazaheri, K., Shafii, M.B., Thermal efficiency improvement of Brayton cycle in the presence of phase change material, *Proceedings of the 9th International Conference of Fluid Flow, Heat and Mass Transfer (FFHMT'22)*, 2022.

[30] Delouei, A.A., Naeimi, H., Sajjadi, H., Atashafrooz, M., Imanparast, M., Chamkha, A.J., An active approach to heat transfer enhancement in indirect heaters of city gate stations: An experimental modeling, *Applied Thermal Engineering*, 237, 2024, 121795.

[31] Hedeshi, M., Jalali, A., Arabkoohsar, A., Amiri Delouei, A., Nanofluid as the working fluid of an ultrasonic-assisted double-pipe counter-flow heat exchanger, *Journal of Thermal Analysis and Calorimetry*, 148(16), 2023, 8579-8591.

[32] Abaszadeh, M., Safavinejad, A., Delouei, A.A., Amiri, H., Analysis of radiative heat transfer in two-dimensional irregular geometries by developed immersed boundary–lattice Boltzmann method, *Journal of Quantitative Spectroscopy and Radiative Transfer*, 280, 2022, 108086.

[33] Abaszadeh, M., Safavinejad, A., Amiri, H., Amiri Delouei, A., A direct-forcing IB-LBM implementation for thermal radiation in irregular geometries, *Journal of Thermal Analysis and Calorimetry*, 147(20), 2022, 11169-11181.

ORCID iD

A. Thilagavathi https://orcid.org/0009-0000-3671-4185
Vallampati Ramachandra Prasad https://orcid.org/0000-0002-9168-3825

© 2024 Shahid Chamran University of Ahvaz, Ahvaz, Iran. This article is an open access article distributed under the terms and conditions of the Creative Commons Attribution-NonCommercial 4.0 International (CC BY-NC 4.0 license) (http://creativecommons.org/licenses/by-nc/4.0/).

How to cite this article: Thilagavathi A., Prasad V.R. Thermal Heat Transfer Enhancement Analysis of Magnetic Ternary Hybrid Nanofluid in a Hexagonal Cavity with Square Obstacle, *J. Appl. Comput. Mech.*, 11(1), 2025, 239-252.
https://doi.org/10.22055/jacm.2024.46544.4548

Publisher's Note Shahid Chamran University of Ahvaz remains neutral with regard to jurisdictional claims in published maps and institutional affiliations.